


Assessment of climate change for predicting water–energy–food–ecosystem nexus vulnerability in a semi-arid basin

Zeynep Özcan ^{a,*}, Toan Trinh^b, M. Levent Kavvas^a and Emre Alp^c

^a Hydrologic Research Laboratory, Department of Civil and Environmental Engineering, University of California, Davis, CA, USA

^b Center for Training and International Cooperation, Vietnam Academy for Water Resources, Hanoi, Vietnam

^c Department of Environmental Engineering, Middle East Technical University, Ankara, Türkiye

*Corresponding author. E-mail: zozcan@ucdavis.edu

 ZÖ, 0000-0002-6140-6771

ABSTRACT

The Water–Energy–Food–Ecosystem (WEFE) nexus highlights the interconnections between water, energy, food, and ecosystems. This study examines climate change's impact on precipitation and temperature in the semi-arid Sakarya Basin, assessing WEFE nexus vulnerability in the 21st century. Climate scenarios (RCP 4.5 and 8.5) from CCSM4 and MIROC5 were downscaled to 18 km grids for three periods (2020–2030; 2055–2065; 2090–2100) using the Weather Research and Forecasting Model (WRF). The assessment integrates these down-scaled data with a range of socio-economic and environmental indicators across seven subbasins. In the most arid, agricultural subbasin, a 22% reduction in precipitation and a 2.9 °C temperature rise are projected. The most populous subbasin may face a 30% precipitation decline and a 3 °C temperature increase. A subbasin, crucial for hydroelectric power, could see a 14% precipitation decrease and a 3 °C temperature rise. These subbasins are identified as the most vulnerable in terms of agricultural productivity, municipal water demand, and energy generation, highlighting significant WEFE nexus challenges. Additionally, the ecosystem sector is highly vulnerable when evaluated against environmental flow parameters. Insights from this study will guide strategies to enhance WEFE nexus resilience in the Sakarya Basin and similar regions under changing climates.

Key words: climate change, dynamical downscaling, regional climate modeling, semi-arid basin, vulnerability assessment, WEFE nexus

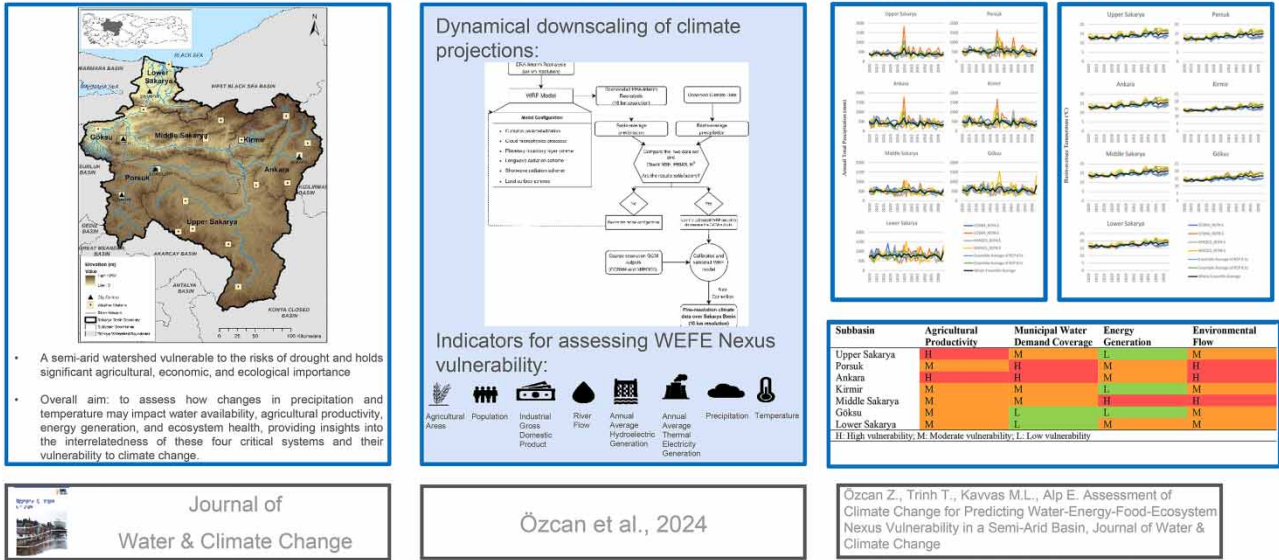
HIGHLIGHTS

- We predict WEFE vulnerabilities using climate and socio-economic indicators.
- WEFE nexus vulnerability is assessed via an integrated multi-indicator approach.
- Vulnerabilities in agriculture, energy, water, and ecosystems vary by subbasin.
- The study guides semi-arid climate impact management.
- Results emphasize the need for integrated strategies to enhance WEFE resilience.

GRAPHICAL ABSTRACT

Assessment of Climate Change for Predicting Water-Energy-Food-Ecosystem Nexus Vulnerability in a Semi-Arid Basin

Tailored climate strategies are essential to safeguard water, energy, food, and ecosystems in semi-arid regions with diverse subbasin characteristics, where climate change impacts vary significantly



Journal of Water & Climate Change

Özcan et al., 2024

Özcan Z., Trinh T., Kavvas M.L., Alp E. Assessment of Climate Change for Predicting Water-Energy-Food-Ecosystem Nexus Vulnerability in a Semi-Arid Basin, Journal of Water & Climate Change

1. INTRODUCTION

The Water–Energy–Food–Ecosystem (WEFE) nexus is an integrated approach that recognizes the interconnections and interdependencies between water, energy, food, and ecosystem sectors (Hanes *et al.* 2018; Garcia *et al.* 2019; Karabulut *et al.* 2019; Momblanch *et al.* 2019; Özcan 2023). As climate change is expected to have significant impacts on these sectors, understanding the potential effects on the WEFE nexus is crucial for the effective management of the nexus components. In this context, analyzing precipitation and temperature at the watershed scale is critical since precipitation and temperature patterns influence the availability and quality of water resources, which are relied upon for various human activities, including agriculture, industry, and energy production. Climate change alters precipitation patterns and temperature regimes at both global and regional scales (Liu 2016), and these changes can lead to more frequent and intense droughts, floods, and other extreme weather events that can have significant impacts on water resources, ecosystems, and human societies (Apeh & Nwulu 2024). At the watershed scale, changes in precipitation patterns can affect the amount and timing of water availability, which can impact the water supply for human consumption, energy generation (Alakbar & Burgan 2024), irrigation, and other uses. Temperature changes can also affect the water balance of a watershed by altering the rate of evapotranspiration, which can impact the amount of water available for use (Wubneh *et al.* 2023).

Analyzing trends in and revealing the climate-change impacts on watershed-scale precipitation and temperature is necessary to understand the effects of climate change on the WEFE nexus. Changes in precipitation and temperature can have significant effects on the availability and distribution of water resources, which can in turn impact food production (FAO 2015), energy generation (Cevik 2022), and ecosystem services (Bates *et al.* 2008). By analyzing trends in precipitation and temperature, we can gain insights into the potential impacts of climate change and develop management strategies to mitigate these impacts. However, there is a lack of a conceptual framework and adequate practices to connect the primary drivers of climate change affecting water resources with the Water–Energy–Food nexus and associated ecosystem processes, which in turn results in knowledge gaps (Liu 2016). Analyzing the impacts of climate change and performing trend analysis on a subbasin scale within a semi-arid watershed is particularly important because climatic characteristics may vary significantly from one subbasin to another. This variability can have significant implications for water availability and usage,

making it crucial to account for these differences in developing effective management strategies. *Ishida et al. (2017)* indicated that when assessing hydrological issues related to climate change, it may be more effective to analyze precipitation across multiple watersheds rather than focusing on just one. This is because the impacts of climate change on precipitation can vary among different watersheds within the same region.

Global climate models (GCMs) simulate climate at a global scale, typically with spatial resolution ranging from tens to hundreds of kilometres. However, this resolution is often insufficient for making predictions at regional or local scales, where climate impacts are felt most acutely (*Xu et al. 2019*). Dynamical downscaling is a technique used to obtain higher-resolution climate projections from GCMs (*Giorgi & Bates 1989*). This technique aims to address this issue by using regional climate models (RCMs) to simulate conditions at higher spatial resolutions, typically ranging from a few kilometres to tens of kilometres (*Giorgi & Gutowski 2015*). Thus, the dynamical downscaling approach can be used whenever small-scale information on future climate or climate change is needed. Consequently, dynamical downscaling finds extensive use in numerous regions and across diverse climate domains (e.g., *Hay & Clark 2003*; *Dulière et al. 2011*; *Soares et al. 2012*; *Erler et al. 2015*; *Ishida et al. 2017*; *Hu et al. 2018*; *Komurcu et al. 2018*). Other downscaling approaches include statistical downscaling, which involves using statistical techniques to relate large-scale climate variables from GCMs to smaller-scale variables at the regional or local level (*Kim et al. 1984*). Statistical downscaling methods are often faster and less computationally intensive than dynamical downscaling methods, but they may not capture the full range of regional climate processes and are less suitable for simulating changes in extreme weather events (*Jang & Kavvas 2015*).

In climate-change impact studies, it is crucial to consider the uncertainties in climate projections. The inertia of the Earth system, along with increased greenhouse gas (GHG) emissions, will lead to further warming in the 21st century, but the degree of this warming remains highly uncertain. This uncertainty is primarily due to three factors: natural variability, model uncertainty, and GHG emission scenario uncertainty (*Latif 2011*). One approach to account for these uncertainties is to include a collection of simulations, known as an ensemble (e.g. *Van Khiem et al. 2014*; *Kaur et al. 2020*; *Dong et al. 2021*; *Gao et al. 2022*).

In this study, we assess climate-change impacts on annual precipitation and temperature across seven subbasins in the semi-arid Sakarya Basin, which is vulnerable to the risks of drought and holds significant agricultural, economic, and ecological importance. This assessment is crucial for predicting vulnerabilities in the WEFE nexus. While the impacts of climate change on basin-scale nexus systems have been previously studied (e.g., *Liu 2016*; *Dlamini et al. 2023*; *Jander et al. 2023*; *Baccour et al. 2024*), our study introduces a distinct approach. We employ a methodology that integrates dynamically downscaled climate data from the Weather Research and Forecasting (WRF) model, specifically calibrated and validated for the Sakarya Basin, with an 18 km spatial and hourly temporal resolution across three future periods (2020–2030, 2055–2065, and 2090–2100). By doing so, we aim to capture both large-scale and small-scale climate dynamics that are critical for understanding localized climate impacts on water, energy, food, and ecosystem sectors. Furthermore, we have incorporated four different climate projections (CCSM4 and MIROC5 under RCP 4.5 and RCP 8.5), enabling us to analyze a wider range of future climate scenarios and uncertainties. After bias correction, we analyze trends in basin-average precipitation and temperature using least squares regression and the Mann–Kendall test, in addition to the statistics, i.e., min, max, and mean, of the basin-average precipitation and temperature based on the annual average precipitation and temperature time-series. The primary aim of this study is to examine the potential impacts of these changes on the nexus sectors' vulnerabilities. These sectors are represented by municipal water demand coverage, energy generation, agricultural productivity, and environmental flow. By incorporating subbasin-specific indicators, we account for variability across the subbasins of the larger Sakarya Basin, allowing for a more localized and precise vulnerability assessment. Our integrated multi-indicator evaluation method combines dynamically downscaled precipitation and temperature data with socio-economic and environmental indicators, i.e., agricultural areas (%), population, provincial gross domestic product (million TL), current state river flow (hm^3/y), annual average hydroelectric generation (GWh), and annual average thermal electricity generation (GWh), all together providing a holistic understanding of how changes in climate patterns will affect the interconnected WEFE sectors at both basin and subbasin scales. Additionally, unlike most studies (e.g., *Wu et al. 2022*; *Albatayneh 2023*; *Dlamini et al. 2023*; *Jander et al. 2023*; *Gao et al. 2024*), we include an ecosystem component, which is essential for sustaining the other nexus sectors.

Finally, our work informs future WEFE nexus studies by providing inputs to integrated water–energy systems models. This contribution is critical for advancing nexus-based resource management and decision-making, particularly in regions like the Sakarya Basin, where water, agricultural, energy, and ecological demands must be balanced under changing climate conditions.

In conclusion, the novelty of this paper lies in the integration of high-resolution climate projections, a multi-indicator evaluation method, and a subbasin-specific approach to assessing the impacts of climate change on the vulnerability of the WEFE nexus in a semi-arid watershed.

2. MATERIALS AND METHODS

2.1. Study area

The Sakarya Basin is located in northwest Türkiye (Figure 1). It constitutes approximately 7% of Türkiye's surface area, with a drainage area of about 63,000 km². Sakarya River, the main tributary of the basin, arises from the Çifteler Sakaryabaşı springs at 800 m elevation in the south of Eskişehir province. Sakarya River flows into the Black Sea in the Karasu district of Sakarya province. The total length of the Sakarya River is 720 km, and the Sakarya Basin has approximately 3.4% of the total water potential of Türkiye. The total population of the basin is around 7.5 million (DSİ 2017) and corresponds to approximately 9% of the total population of Türkiye. The Sakarya Basin has a wide elevation band, ranging from 0 m on the Western Black Sea coast to 2,510 m on the Uludağ mountain. According to CORINE 2018 data (European Environment Agency 2018), 53% of the Sakarya Basin consists of agricultural areas. Forest and semi-natural areas account for approximately 44%. Artificial surfaces, on the other hand, constitute only about 3% of the total area.



Figure 1 | Geographic location and topography of the Sakarya Basin in Türkiye, represented by a digital elevation map with subbasin boundaries.

The Sakarya Basin has an average annual precipitation of 479 mm and is thus one of four basins in Türkiye with an average rainfall of less than 500 mm. On the other hand, considering the total annual precipitation, it is one of the basins receiving the highest precipitation at 32 billion m³. Additionally, the Sakarya Basin is one of the highest flow-value basins with an annual flow of 12 billion m³, despite being one of the lowest in terms of rainfall per capita (4,437 m³/person) due to its high population (SYGM 2022).

Within the Sakarya Basin, there are seven subbasins: Upper Sakarya, Porsuk, Ankara, Kirmir, Middle Sakarya, Göksu, and Lower Sakarya, listed from upstream to downstream. The selection of the Sakarya Basin for this analysis is primarily due to the unique climatic and socio-economic characteristics exhibited by its subbasins. Each subbasin presents distinct features that highlight different aspects of the WEFÉ nexus. This diversity allows for the application of a uniform methodology across regions that demonstrate varying dynamics and challenges. Table 1 provides details on the drainage area, average precipitation, and average temperature values for each subbasin. These average precipitation and temperature values are derived from observed data collected from September 2009 to September 2018.

A study conducted by the Ministry of Forestry and Water Affairs General Directorate of Water Management in 2016 investigated the potential impacts of climate change on water resources in Türkiye (The Ministry of Forestry & Water Affairs 2016). This study discusses the results of three different climate models (HadGEM2-ES, MPI-ESM-MR, and CNRM-CM5.1) and their projections for the Sakarya Basin in Türkiye. The models predict an increasing trend in temperature values during the projection period compared with the reference period. The models also predict changes in precipitation, with the possibility of both increases and decreases, although a decrease in precipitation is expected to be dominant. The study shows that rising temperatures and changing precipitation patterns have led to a decline in streamflow and groundwater recharge. The findings have important implications for water resource management in the country and highlight the need for adaptation strategies to cope with the impacts of climate change.

In the semi-arid Sakarya Basin, known for its high population density, agricultural significance, and intensive industrial activities, investigating the effects of climate change and implementing appropriate measures is crucial. Moreover, the basin's climate varies significantly from north to south, making it crucial to evaluate the impact of climate change on precipitation and temperature at the subbasin level for effective adaptation.

2.2. Methodology

The Sakarya Basin is divided into seven subbasins, each with unique characteristics and vulnerabilities to climate-change impacts on the WEFÉ nexus. To predict the WEFÉ nexus vulnerability, we employed an integrated multi-indicator evaluation approach. This method integrates dynamically downscaled climate data with a comprehensive set of socio-economic and environmental indicators. Specifically, we used historical data for the WEFÉ nexus and future projections for climate variables.

2.2.1. Methodology for dynamical downscaling for high-resolution climate projections

The future climate data were obtained by dynamical downscaling through WRF, a regional climate model. Figure 2 shows the flow diagram of the methodology followed to obtain the fine-resolution future climate data in the Sakarya Basin. As can be seen from the figure, the WRF model needs to be calibrated first before downscaling the GCM outputs to the desired resolution. For this purpose, first, ERA-Interim reanalysis data with a spatial resolution of 80 km were obtained. Then, ERA-

Table 1 | Summary of subbasin characteristics including drainage area, average precipitation, and average temperature

	Drainage area (km ²)	Average precipitation (mm)	Average temperature (°C)
Upper Sakarya	21,325	380	12.2
Porsuk	10,722	479	11.8
Ankara	7,178	417	12.4
Kirmir	4,600	458	13.6
Middle Sakarya	12,106	496	13.1
Göksu	2,435	531	13.5
Lower Sakarya	4,738	733	15.9

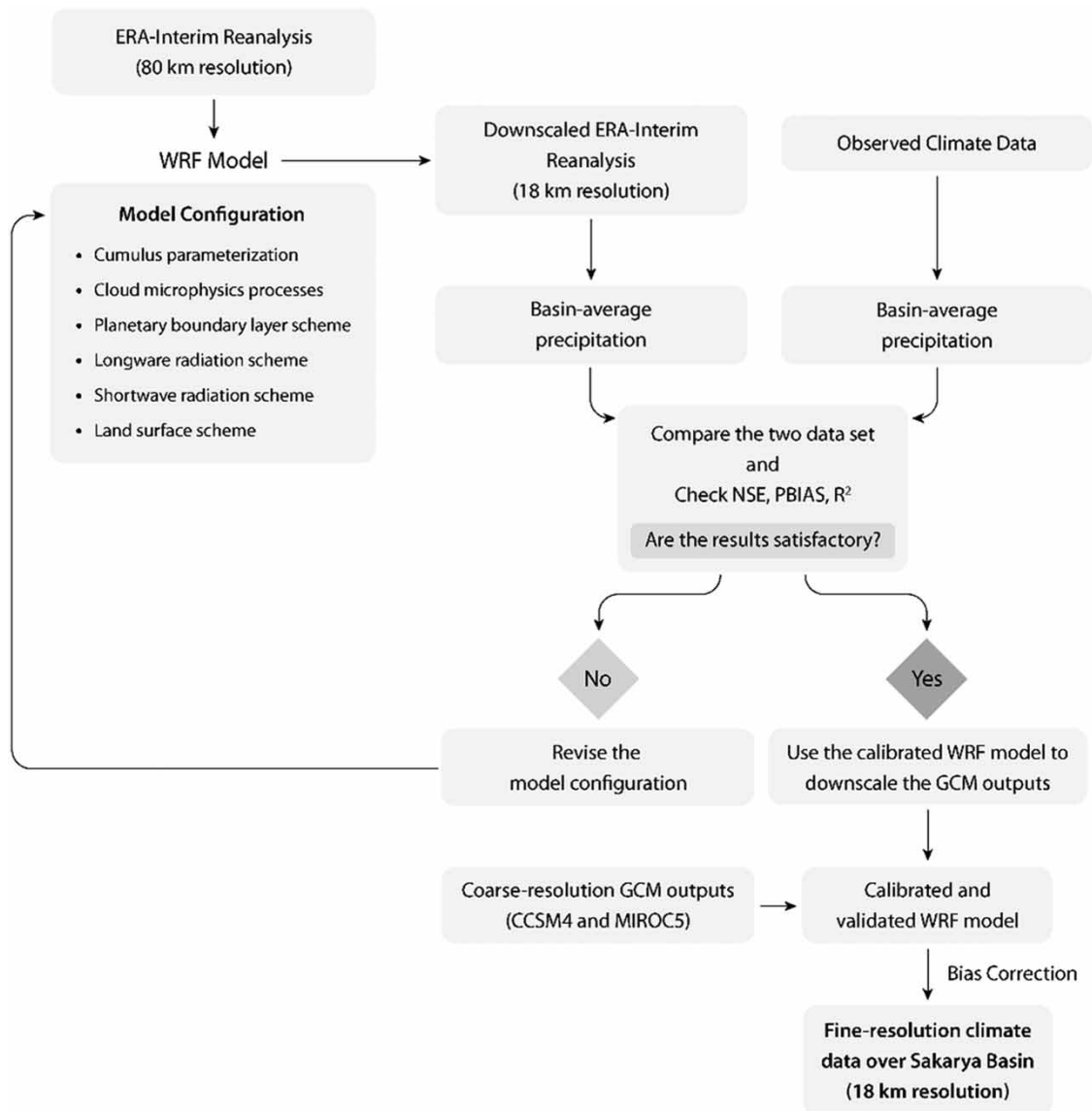


Figure 2 | Flow diagram of the methodology to obtain fine-resolution climate data in the Sakarya Basin.

Interim reanalysis data were downscaled in different model configurations until a satisfactory model performance was obtained. Whether the model performance is satisfactory or not was evaluated by comparing the basin-average values of the downscaled ERA-Interim data and the basin-average values of the observed data. When satisfactory model performance was achieved, the calibrated and validated WRF model was used to downscale the GCM outputs to a resolution of 18 km. After correcting the bias in the downscaled GCM outputs, the future climate data took its final form and trend analysis was performed on watershed-scale precipitation and temperature.

Climate change was analyzed in terms of the projected changes and trends in the basin's average annual total precipitation depths and basin-average temperatures over the seven study subbasins in the Sakarya Basin in the 21st century. The future period was divided into three segments as near century (2020–2030), mid-century (2055–2065), and far century (2090–2100), for a total of 33 years. The results were investigated based on the four dynamically downscaled bias-corrected future climate projections accordingly. In addition to the individual assessment of all climate projection realizations, the analysis was also performed based on the ensemble averages of two emission scenarios (RCP 4.5 and RCP 8.5) and the ensemble average of all GCMs (CCSM4 and MIROC5). Ensemble averages are useful for the assessment of the general trends in the

precipitation and temperature, and to take into account the uncertainties resulting from the selected GCMs and scenarios (Ishida *et al.* 2020).

The least squares regression method and the Mann–Kendall trend test were employed to quantify the trends in the annual basin-average precipitation and temperature. The slopes and the standard errors of the trend lines were calculated through the least squares regression method. The Mann–Kendall trend test is non-parametric and it is used to determine the significance of consistently increasing or decreasing trends (Mann 1945).

2.2.2. Methodology for evaluating WEFE nexus vulnerability

This study follows an indicator-based approach to assess the vulnerability of the WEFE nexus components in the study sub-basins. Figure 3 illustrates the overall methodology. Using an indicator-based approach is common in WEFE nexus assessment studies (e.g. Giupponi & Gain 2017; Saladini *et al.* 2018; Momblanch *et al.* 2019; Yuan & Lo 2020). These studies differ in the components they address, their scale, and the number of indicators used. Indicators are typically defined based on resource availability, accessibility, self-sufficiency, and productivity. Nhamo *et al.* (2020) emphasize excluding indicators unrelated to these drivers while Endo *et al.* (2015) stress the importance of linking indicators closely to measurement objectives and tailoring them to the specific research area. Thus, in this study, the selection of indicators considered the major drivers of WEFE nexus security, the characteristics of the study basin, and data availability.

Table 2 presents a selection of indicators for assessing the vulnerability of the WEFE nexus in the study subbasins. These indicators encompass both climate-related variables and socio-economic factors. To assess WEFE nexus vulnerability, we used historical socio-economic data under the assumption of a ‘business-as-usual’ scenario, assuming current socio-economic conditions would remain stable. This approach provides a baseline for evaluating the effects of climate variability and change while simplifying the analysis by focusing on climate impacts. In assessing the vulnerabilities of WEFE nexus sectors, represented, respectively, by agricultural productivity, municipal water demand coverage, energy generation, and environmental flow, we conducted expert judgment evaluations. These assessments, specific to each subbasin, were based on statistically analyzed climate data obtained through dynamic downscaling and socio-economic indicators reflecting sectoral importance across subbasins. Instead of direct quantitative calculations, insights were derived through a synthesis of climate data analyses and socio-economic indicators to infer sectoral vulnerabilities.

2.3. Data and model implementation for dynamical downscaling

This study uses four different future climate projection realizations from two general circulation models (GCMs: CCSM4 and MIROC5) based on two emission scenarios (RCP 4.5 and RCP 8.5). CCSM4 is the fourth version of the Community Climate System Model (CCSM4) (Gent *et al.* 2011). The model was developed by the National Center for Atmospheric Research (NCAR), United States. It has a spatial resolution of $0.9^\circ \times 1.25^\circ$. MIROC5 is the latest version of the Model for Interdisciplinary Research on Climate which was cooperatively produced by the Japanese research community (Watanabe *et al.* 2010). The model has a spatial resolution of $1.4^\circ \times 1.4^\circ$. The two emission scenarios selected were RCP 4.5 and RCP 8.5.

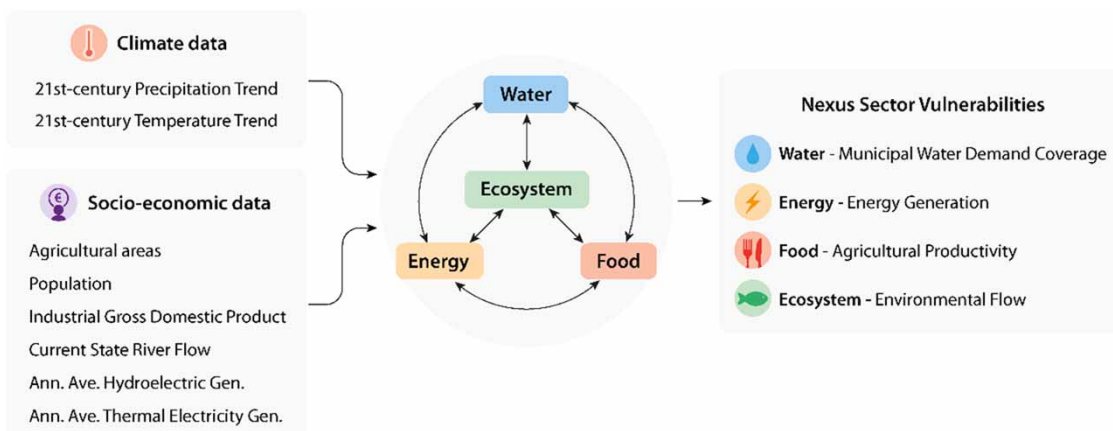


Figure 3 | Overview of the methodology for assessing vulnerabilities across nexus sectors.

Table 2 | Indicators for assessing WEFE nexus vulnerability

Indicator name	Indicator description
Agricultural areas (%)	Agricultural areas (%) (European Environment Agency 2018) indicate land dedicated to agriculture, vital for assessing water and food security.
Population	Population size (–) (DSİ (2017)) impacts water and energy consumption and food demand, essential for predicting future pressures on the WEFE nexus.
Industrial gross domestic product (million TL)	The provincial gross domestic product (million TL) (T.C. Sanayi ve Teknoloji Bakanlığı (2020)) serves as a proxy for economic activity, influencing resource consumption patterns.
Current state river flow (hm ³ /y)	Current state river flow (hm ³ /y) (DSİ (2017)) is critical for assessing water availability and its implications for energy generation and agricultural irrigation, providing a baseline for understanding hydrological changes.
Annual average hydroelectric generation (GWh)	Annual average hydroelectric generation (GWh) (DSİ (2022)) represents the energy produced from hydroelectric sources, directly linking energy production to water availability.
Annual average thermal electricity generation (GWh)	Annual average thermal electricity generation (GWh) (Enerji Atlası (2023)) reflects energy output from water-dependent thermal plants, highlighting water–energy interdependencies and vulnerabilities due to substantial water requirements.
21st-Century precipitation trend	The 21st-century precipitation trend captures long-term shifts in precipitation patterns, reflecting potential changes in water availability critical for agriculture, energy production, and ecosystem health.
21st-Century temperature trend	The 21st-century temperature trend indicates changes in average temperatures over time, a critical factor affecting water demand, crop viability, and energy consumption.

RCP 4.5 is a scenario that stabilizes radiative forcing at 4.5 W m^{-2} in the year 2100 without ever exceeding that value ([Thomson *et al.* 2011](#)). On the other hand, the GHG emissions and concentrations in the RCP 8.5 scenario increase considerably over time, leading to a radiative forcing of 8.5 W/m^2 at the end of the century. RCP 8.5 corresponds to the pathway with the highest GHG emissions compared with the total set of RCPs ([Riahi *et al.* 2011](#)).

It is necessary to downscale the GCM results to finer spatial resolutions for a reliable assessment of the regional impact of climate change on precipitation and temperature. Dynamical downscaling is one of the techniques to do this by means of an RCM. In this study, the WRF model is used to dynamically downscale future climate projection realizations. The WRF model is a mesoscale numerical weather prediction system designed for both atmospheric research and operational forecasting applications, developed collaboratively by multiple agencies ([Skamarock *et al.* 2008](#)). It is a fully compressible and non-hydrostatic model.

In this study, the future projection period ranges from 2020 to 2100. The future climate projection realizations were downscaled to 18 km resolution grids over the Sakarya Basin for a period of 33 years (2020–2030; 2055–2065; 2090–2100). The realizations were downscaled as ten-year segments due to the high computational cost of the regional model and time constraints. The historical atmospheric data used in this study is from September 2009 to September 2018 based on the availability of observed meteorological data in the study basin. Observed daily total precipitation and temperature data from 20 different meteorological stations within the Sakarya Basin were obtained from the Turkish State Meteorological Service (MGM). These stations are detailed in [Table 3](#) and their geographic locations are illustrated in [Figure 1](#).

2.4. WRF model calibration and validation

Before downscaling future climate projections, the WRF model needs to be calibrated. ERA-Interim reanalysis data was used for the calibration of the model. ERA-Interim is one of the best reanalysis datasets of its generation and has been extensively downscaled with WRF. It is a common practice to use ERA-Interim-driven WRF simulations to evaluate the ability of the WRF model to simulate observed fields ([Gorguner *et al.* 2019](#)). For this purpose, reanalysis data for the years between 2009 and 2018 were obtained. ERA-Interim data set with a 6 h temporal resolution is available from the Research Data Archive (RDA) at NCAR. The spatial resolution of the dataset is approximately 80 km with 60 levels in the vertical from the surface up to 0.1 hPa.

Before downscaling the ERA-Interim reanalysis for the entire historical period, the WRF model was first calibrated for the year 2010 by comparing its results to the observed total monthly precipitation data. The observed data from 20 different

Table 3 | Details of the meteorological stations in the Sakarya Basin used in this study

Station number	Station name	Latitude	Longitude	Automatic measurement period
17753	BAYAT	38.9715	30.9179	2005–2018
17798	YUNAK	38.8205	31.7258	2009–2018
17680	BEYPAZARI	40.1608	31.9172	2005–2018
17662	GEYVE	40.5214	30.296	2005–2018
17644	KARASU	41.1113	30.6901	2006–2018
17155	KUTAHYA	39.4171	29.9891	2005–2018
17723	CIFTELER	39.3659	31.0209	2005–2018
17752	EMIRDAG	39.0098	31.1463	2005–2018
17832	ILGIN	38.2763	31.894	2009–2018
17728	POLATLI	39.5834	32.1624	2005–2018
17733	HAYMANATARIM	39.613	32.672	2005–2018
17128	ANKARA ESENBAGA	40.124	32.9992	2005–2018
17693	SEBEN	40.4088	31.573	2005–2018
17664	KIZILCAHAMAM	40.4729	32.6441	2005–2018
17130	ANKARABOLGE	39.9727	32.8637	2005–2018
17118	BURSA YENISEHIR	40.2552	29.5624	2009–2018
17069	SAKARYA	40.7676	30.3934	2005–2018
17126	ESKISEHIR BOLGE	39.7656	30.5502	2005–2018
17120	BILECIK	40.1414	29.9772	2005–2018
17679	NALLIHAN	40.1733	31.332	2005–2018

meteorological stations were used to calculate the basin's average total monthly precipitation. For this purpose, the Thiessen polygon method was used. Two two-way nested domains were set up for the WRF dynamical downscaling, as shown in Figure 4. The outer domain (D01) has 31×33 horizontal grid points at a 54 km resolution, and the second domain (D02) has 28×25 horizontal grid points at an 18 km resolution with 25 vertical (Eta) levels. The outer domain, D01, comprises southeast Europe, the Black Sea, the Aegean Sea, and the eastern Mediterranean Sea. The second domain, D02, comprises the whole Sakarya Basin.

To find the best combination of physics options, several different combinations of the parameterizations of the WRF model were tested. The model configuration of the WRF model used in this study is shown in Table 4.

After the WRF model was calibrated for the year 2010, the model was validated for the years from 2009 to 2018 by comparing the total basin averaged monthly precipitation with the observed values (Figure 5). A statistical summary of the calibration and validation results is listed in Table 5. For the assessment of model performance, mean (mm), standard deviation (mm), coefficient of variation of the modeled and observed time-series, correlation coefficient, Nash–Sutcliffe model efficiency (NSE), Percent Bias (PBIAS), and coefficient of determination (R^2) were employed. As can be seen from Table 5, the statistical parameters indicate satisfactory model simulations. The calibrated and validated WRF model was then used to downscale the climate projections of CCSM4 and MIROC5 under RCP 4.5 and RCP 8.5 scenarios to a spatial resolution of 18 km.

2.5. Bias correction methodology for climate outputs

To correct biases, the delta change method was used as it is the simplest approach for bias correction. In this approach, a time series of future climate is generated (Maraun 2016):

$$x_{i,\text{corr}}^f = x_{i,\text{raw}}^f - \text{Bias}(\mu^p) = x_{i,\text{raw}}^f - (\bar{x}_i^p - \bar{y}_i^p) \quad (1)$$

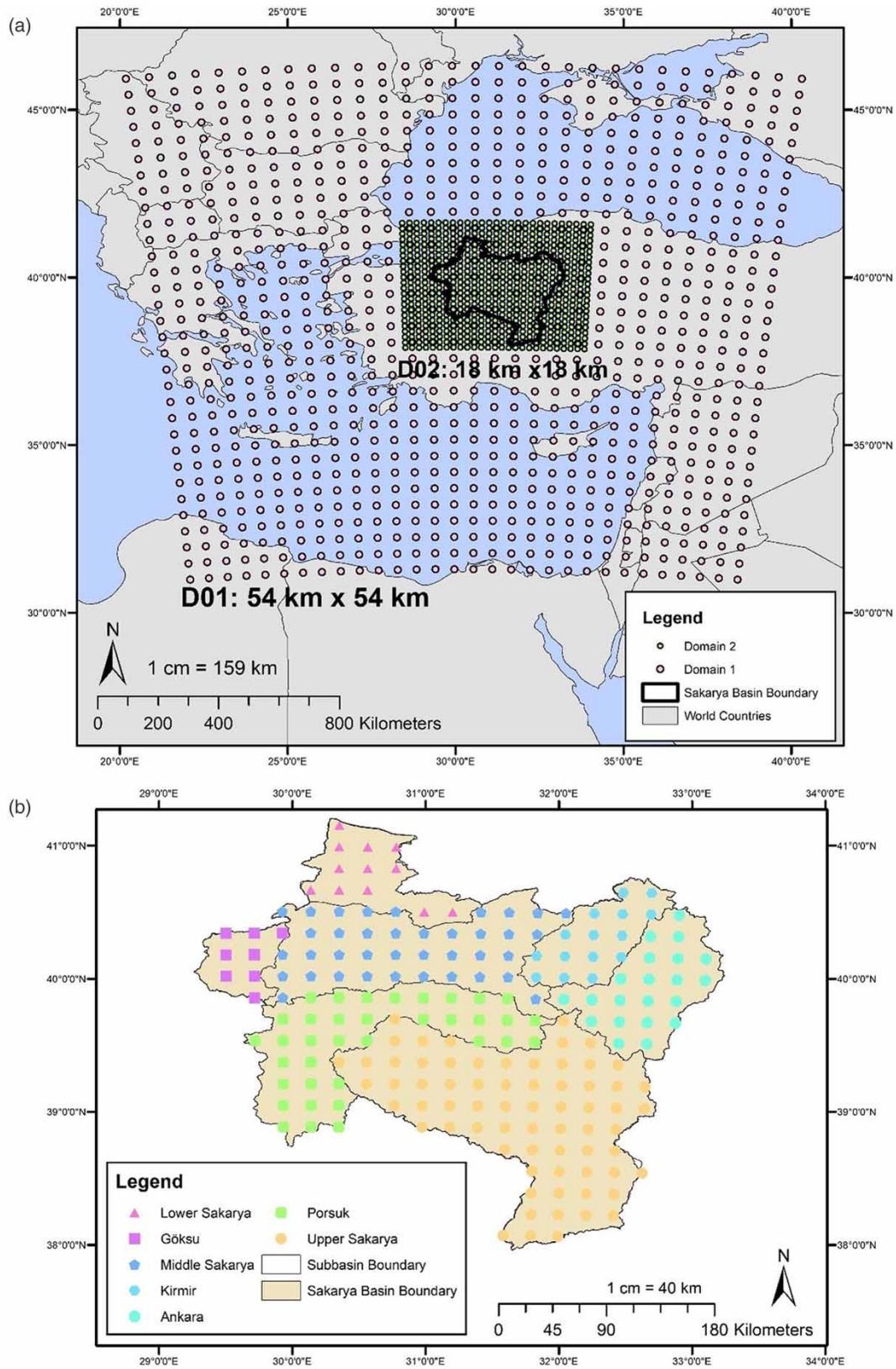


Figure 4 | (a) Nested WRF domain configuration over the Sakarya Basin and (b) grid points used to calculate the basin-average precipitation and temperature values for each subbasin.

Table 4 | WRF model configuration

Cumulus parameterization	Grell-3D scheme (an improved version of the GD scheme) (Grell & Dévényi (2002))
Cloud microphysics processes	Kessler (Kessler 1969)
Planetary boundary layer scheme	Yonsei University (Hong <i>et al.</i> 2006)
Longwave radiation scheme	RRTM scheme (Mlawer <i>et al.</i> 1997)
Shortwave radiation scheme	Dudhia (Dudhia 1989)
Land surface scheme	Rapid Update Cycle (RUC) land surface model (Smirnova <i>et al.</i> 1997)

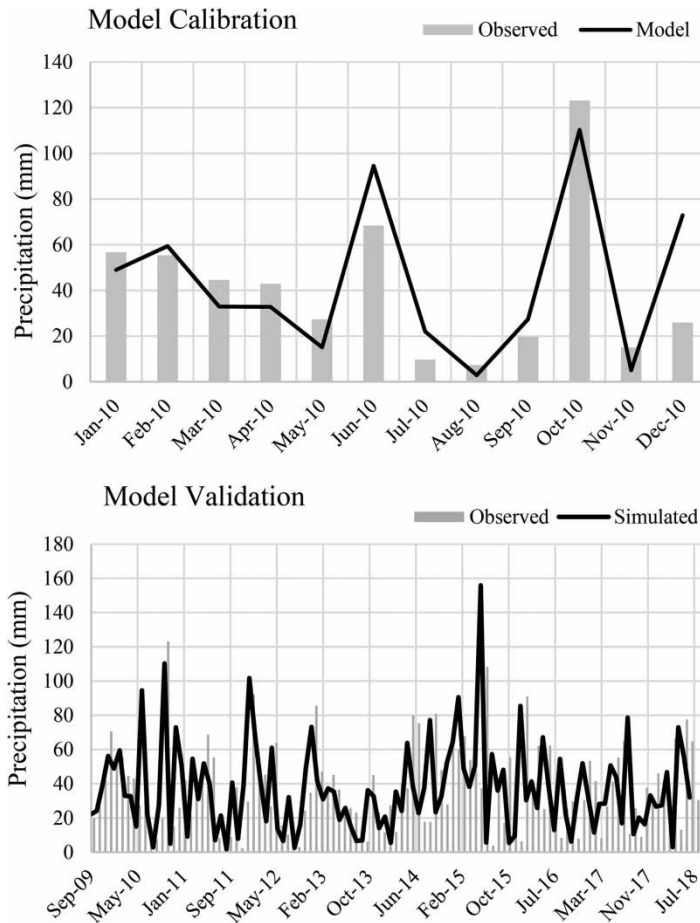


Figure 5 | Calibration and validation results for the WRF model.

or equivalent for precipitation:

$$x_{i,corr}^f = \frac{x_{i,raw}^f}{Rel.Bias(\mu^P)} = x_{i,raw}^f \frac{\bar{y}_i^p}{\bar{x}_i^p} \tag{2}$$

where x_i^p is a simulated present-day model (predictor) time series of length N ; y_i^p is the corresponding observed (predictand) time series; $x_{i,corr}^f$ is the corrected future simulations; $x_{i,raw}^f$ is the raw future simulations

Table 5 | Statistical summary of the calibration and validation results

	Calibration	Validation
Mean (mm)		
Model	43.7	36.9
Observation	41.3	37.8
Standard deviation (mm)		
Model	34.5	26.1
Observation	32.5	24.6
Coefficient of variation		
Model	0.790	0.708
Observation	0.786	0.652
Correlation coefficient	0.848	0.844
Nash–Sutcliffe coefficient	0.669	0.664
PBIAS	−5.62	2.21

The GCM (CCSM4 and MIROC5) precipitation and temperature projections from September 2009 to July 2018 were downscaled, based on the availability of observed data in the monitoring stations, and the observed and downscaled basin-average monthly precipitation and temperature values were calculated. Then, Equation (1) and Equation (2) were used to correct biases in temperature and precipitation, respectively.

3. RESULTS AND DISCUSSION

In this section, we explore the projected changes and trends in basin-average precipitation and temperature in the 21st century. Additionally, we assess the vulnerability of the WEFE nexus in seven study subbasins, taking into account both climate and socio-economic factors. This comprehensive analysis is structured as follows: annual total basin-average precipitation (3.1), basin-average temperature (3.2), and WEFE nexus vulnerability (3.3).

3.1. Projected changes and trends in annual total basin-average precipitation in the 21st century

Temporal variability of annual total basin-average precipitation over the seven subbasins for all four climate projection realizations, the ensemble averages of RCP 4.5 and RCP 8.5 scenarios, and the ensemble averages of all realizations are shown in Figure 6. As it can be seen from Figure 6, no clear significant increasing or decreasing trend is observed for annual total precipitations in the 21st century in all subbasins. However, there are some peaks evident especially in the mid-century. The slopes and standard errors of the least squares regression line of annual basin-average precipitation depths over the seven study subbasins with *p*-value of the Mann–Kendall trend test in parentheses are given in the Supplementary Material, Tables A1–A4 of Appendix A for the 21st century, near century, mid-century, and far century, respectively. In these tables, the *p*-values are bolded if the trend is statistically significant at the 95% confidence level.

Minimum and maximum values of annual total precipitation depths in the historical period as well as in the 21st century and each segment of the future period over the seven study subbasins with the mean value in parentheses are given in the Supplementary Material, Tables A1–A4, respectively. Statistical information about the historical period was provided for comparison purposes. The given mean values in these tables indicate the average of the annual total precipitation depth for the relevant time-period. In this way, the changes in the precipitation depths are analyzed by comparing the historical means with the means of each future-period segment. Additionally, the Supplementary Material, Figure B1 in Appendix B presents box-and-whisker plots of total monthly precipitation for the ensemble average across each subbasin.

In the Upper Sakarya subbasin, all climate projection realizations except for CCSM4_RCP8.5 and the ensemble of RCP 8.5 scenarios show a decreasing trend in the basin-average precipitation in the 21st century. Among all of the projections, only the trend in the ensemble of RCP 4.5 scenarios is statistically significant. In the near century, while all CCSM4 projections and the ensemble of RCP 8.5 scenarios have an increasing trend, the rest of the projections have a decreasing trend. However, none of the trends is statistically significant. Similar to the trends in the near century, there is no statistically significant trend

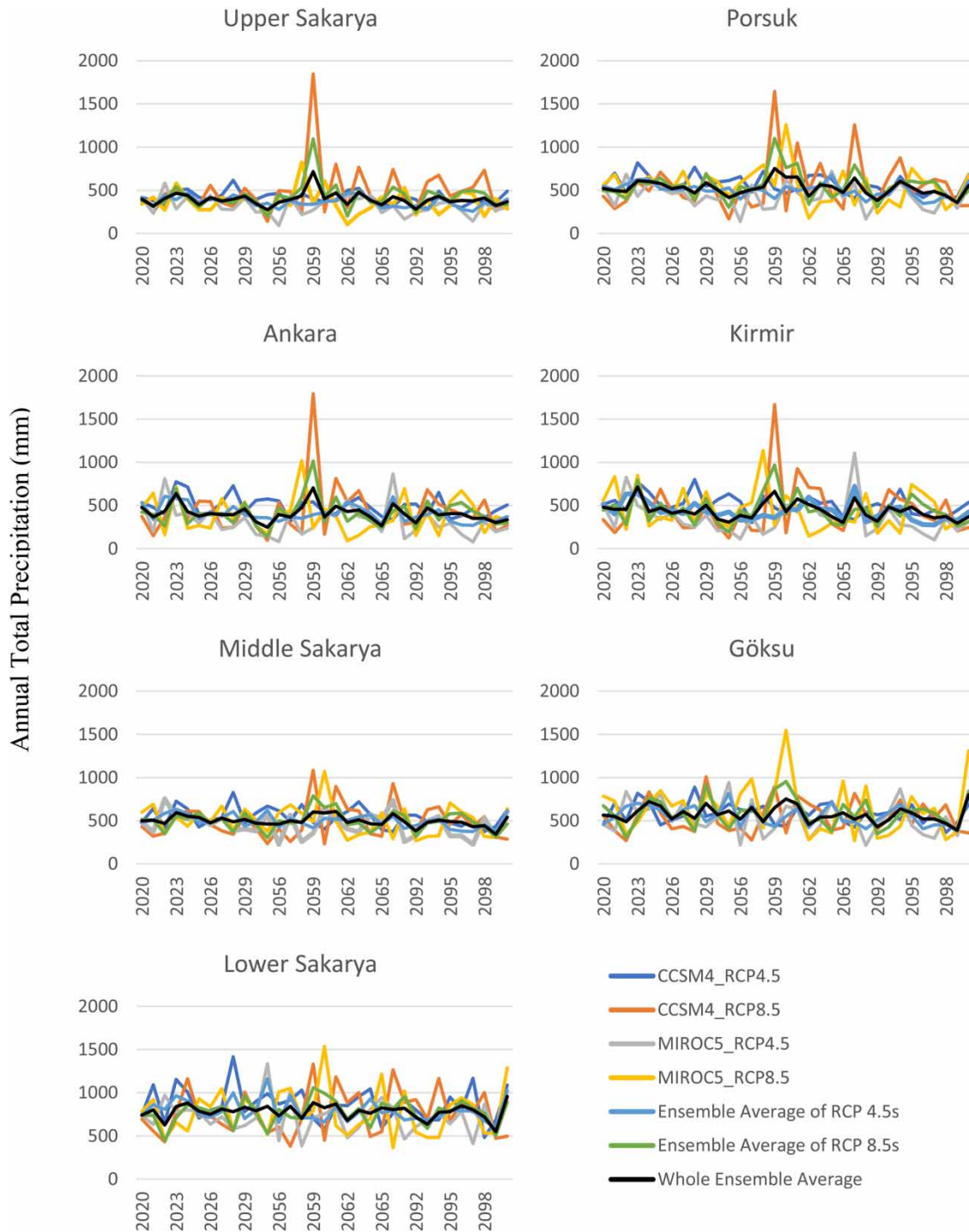


Figure 6 | Annual total basin-average precipitation over the seven subbasins: Upper Sakarya, Porsuk, Ankara, Kirmir, Middle Sakarya, Göksu, Lower Sakarya. All four climate projection realizations, the ensemble averages of RCP 4.5 scenarios, the ensemble averages of RCP 8.5 scenarios, and the ensemble averages of all realizations are shown.

in the mid-century. Three of the projections, i.e., CCMS4_RCP4.5, MIROC5_RCP8.5, and the ensemble of RCP8.5 scenarios have a decreasing trend while the rest have an increasing trend. Finally, all RCP 8.5 projections and the ensemble of all projections indicate a decreasing trend in the far century. Again, the trends are away from the monotonic trend according to the

p-value of the Mann–Kendall trend test. When the statistics of the historical precipitation are compared with the 21st century, near, mid-, and far century, the mean of the MIROC5 projections and the mean of the ensemble of RCP 4.5 scenarios are lower compared with the historical period with the only exception being the ensemble of RCP 4.5 in the near century. The lowest mean is projected in the MIROC5_RCP 4.5 in all periods.

In the Porsuk subbasin, the only projection with an increasing trend in the 21st century is the CCSM4_RCP8.5 but the trend is not monotonic. All of the ensembles, all MIROC5 projections, and the CCSM4_RCP4.5 scenario have a decreasing trend. Furthermore, CCSM4_RCP4.5 and the ensemble of RCP4.5 denote a statistically significant decreasing trend. In all of the three segments of the future period, although the trends are either decreasing or increasing depending on the GCM and the RCP involved, there is no significant trend in the time series. From the Supplementary Material, Tables A1 to A4, it can be seen that the only projection with a lower mean as compared with the historical period is MIROC5_RCP4.5, though in the far century the ensemble of RCP 4.5 scenarios also projects a lower mean. Among all projections, the lowest mean in the Porsuk subbasin is projected by MIROC5_RCP4.5 in all periods.

The Mann–Kendall trend test detected a significant downward trend in the CCSM4_RCP4.5 and the ensemble average of RCP 4.5 scenarios in the Ankara subbasin in the 21st century. All of the projections except for CCSM4_RCP4.5 show a decreasing trend in the near century. However, none of these trends are statistically significant. Similarly, there is no significant upward or downward trend in the climate projections either in the mid- or far century. Although the trends are either increasing or decreasing in the mid-century, all of the projections indicate a decreasing trend in the far century. In the Supplementary Material, Tables A1–A4 show that the means of the CCSM4_RCP4.5, MIROC5_RCP4.5, MIROC5_RCP8.5, the ensemble of RCP 4.5s, the ensemble of RCP 8.5s and the ensemble of all projections are lower than the mean of the historical period both in the 21st century and the far century. In the near and mid-century, the results are similar to the 21st century and the far century with the only exception being that the ensemble of RCP 4.5 scenarios projects a higher mean in comparison with the historical period. The basin-average annual total precipitation resulting from the MIROC5_RCP4.5 scenario is the lowest among all other projections in all periods.

In the Kirmir subbasin, all the climate projections except for CCSM4_RCP8.5 have a decreasing trend in the 21st century. Moreover, three of these downward trends, i.e., CCSM4_RCP4.5, the ensemble of RCP 4.5s, and the ensemble of all projections, are statistically significant. The results in the near century are very similar to the Ankara subbasin. The only difference is that the downward trend in the MIROC5_RCP4.5 scenario is close to the monotonic trend. This is the only projection that has a statistically significant trend among all projections in all study subbasins in the near century. The number of climate projections with an upward trend in the mid-century is higher compared with the ones with a downward trend. However, none of them has statistically significant *p*-values. Finally, in the far century, only two of the projections have an increasing trend while the rest have a decreasing trend. Again, there is no monotonic trend. When the mean precipitation values of the historical and future periods are compared, it is seen that all the projections except for CCSM4_RCP4.5 project a lower mean than the historical period in the 21st century and the far century. In the near century, the mean values are lower in the CCSM4_RCP8.5, MIROC5_RCP4.5, the ensemble of RCP 4.5 scenarios, and the ensemble of all projections. In the mid-century, the results are similar to those of the near century and the only difference is that the MIROC5_RCP8.5 has also a lower mean as compared with the historical period in the mid-century.

In the Middle Sakarya subbasin, all the projections except for CCMS4_RCP8.5 have a decreasing trend in the 21st century. Furthermore, the ensemble average of RCP 4.5 scenarios shows a statistically significant downward trend. In the near and mid-century there is no statistically significant upward or downward trend. There are four downward trends in the near century while there are only two in the mid-century. In the far century, on the other hand, CCSM4_RCP8.5 projection denotes a downward trend with a statistically significant *p*-value. There is no statistically significant evidence that a trend is present in the other climate projections in the far century. In the 21st century and mid-century, CCSM4_RCP8.5 and MIROC5_RCP4.5 projections have lower means as compared with the historical period. In the near century, the ensemble of RCP 8.5 scenarios is also projected to have a lower mean in addition to the CCSM4_RCP8.5 and MIROC5_RCP4.5 projections. Finally, in the far century, all of the climate projections except for CCSM4_RCP8.5 have lower means than the historical period. The lowest mean among all other projections is projected by MIROC5_RCP4.5 in the 21st century, mid- and far century. In the near century, CCSM4_RCP8.5 has the lowest mean as compared with the other projections.

In the Göksu subbasin, none of the climate projections has a significant trend in the 21st century or any segments of the future period. The most remarkable result is that all projections except MIROC5_RCP4.5 are in an increasing trend in the near and far centuries. Göksu is the only subbasin where almost all of the climate projections indicate an increasing trend

in the near and far century but none of them are statistically significant. However, in the mid-century, basin-average annual total precipitation depths tend to decrease. In the 21st century, the only projection that has a lower mean than the historical period is MIROC5_RCP4.5. All of the climate projections in the near century project higher means in comparison with the historical mean. In the mid-century, CCSM4_RCP8.5 and MIROC5_RCP4.5 have lower means as compared with the historical period. In the far century, on the other hand, the means of all projections involving the RCP 4.5 scenario and the ensemble of all scenarios are lower than in the historical period.

Similar to the Göksu subbasin, the Lower Sakarya subbasin does not have any statistically significant p -value in any future period. Only two out of seven projections are on an upward trend in the 21st century. In the near and far century, however, the number of projections with an increasing trend is higher compared with the ones with a decreasing trend. Unlike the near and far century, most of the projections have a downward trend in the mid-century. In the 21st century and mid-century, MIROC5_RCP4.5 is the only projection that has a lower mean compared with the historical mean. In the near century, two of the projections, i.e., CCSM4_RCP8.5 and MIROC5_RCP4.5, project lower means than the historical period. Finally, in the far century, all MIROC5 projections indicate lower means than the mean of the historical precipitation. Moreover, MIROC5_RCP4.5 always projects the lowest mean as compared with the other projections in the Lower Sakarya subbasin.

The results show that all the climate projections with a statistically meaningful p -value point to a downward trend in the basin-average annual total precipitation depths over all study subbasins in the 21st century. There is no projection with an upward trend and with a significant p -value. Thus, the precipitation depths tend to decrease in all subbasins in the 21st century. Except for the Göksu and Lower Sakarya subbasins, there are at least one or more projections with statistically significant decreasing trends in all other subbasins. In addition, Göksu and Lower Sakarya have different trends compared with the other subbasins in all segments of the future period. The CCSM4_RCP8.5 projection, two MIROC5 projections and the ensemble averages of the RCP 8.5 scenarios do not have a significant decreasing or increasing trend based on the results of the Mann–Kendall trend test in any of the subbasins. The p -values of the CCSM4_RCP4.5 projections in the Porsuk, Ankara, and Kirmir subbasins indicate a significant decreasing trend. Similarly, the ensemble averages of the RCP 4.5 scenarios point out a significant decreasing trend in the basin-average annual total precipitation depths of the Upper Sakarya, Porsuk, Ankara, Kirmir, and Middle Sakarya subbasins. Finally, the p -values of the ensemble average of climate projection realizations show a significant decreasing trend only in the Kirmir subbasin. The Mann–Kendall trend test results show neither increasing nor decreasing trend in any of the projections in two subbasins: Göksu and Lower Sakarya.

In the near century, only one subbasin, i.e., Kirmir, has a projection with a statistically significant decreasing trend, which is MIROC5_RCP4.5. In all subbasins except for Porsuk, Göksu, and Lower Sakarya, the number of projections with a decreasing trend is higher than the number of projections with an increasing trend. In the mid-century, there are no projections with a statistically meaningful p -value. Except for Göksu and Lower Sakarya, the number of projections with an increasing trend is higher than the number of projections with a decreasing trend in all subbasins. Finally, in the far century, there is only one projection, i.e., CCSM4-RCP8.5, with a statistically significant decreasing trend, and this trend is projected in the Middle Sakarya subbasin.

3.2. Projected changes and trends in basin-average temperature in the 21st century

Temporal variability of basin-average temperatures based on the annual average temperature time-series over the seven subbasins for all four climate projection realizations, the ensemble averages of RCP 4.5 and RCP 8.5 scenarios, and the ensemble averages of all realizations are shown in Figure 7. The most obvious conclusion drawn from this figure is that temperatures are on an increasing trend in all subbasins throughout the 21st century. The slopes and standard errors of the least squares regression line of basin-average temperature over the seven study subbasins with a p -value of the Mann–Kendall trend test in parentheses are given in the Supplementary Material, Appendix A in Tables A5–A8 for the 21st century, near century, mid-century, and far century, respectively. The bolded p -values in these tables mean that the trend is statistically significant at the 95% confidence level.

Minimum and maximum values of basin-average temperature in the historical period, as well as in the 21st century and each segment of the future period, over the seven study subbasins with the mean value in parentheses are given in the Supplementary Material, Tables A5–A8, respectively. The statistical information about the historical period was provided for comparison purposes. In these tables, the mean value shows the average of the basin-scale temperatures for the related period. In this way, the changes in the basin-scale temperatures are analyzed by comparing the historical means with the

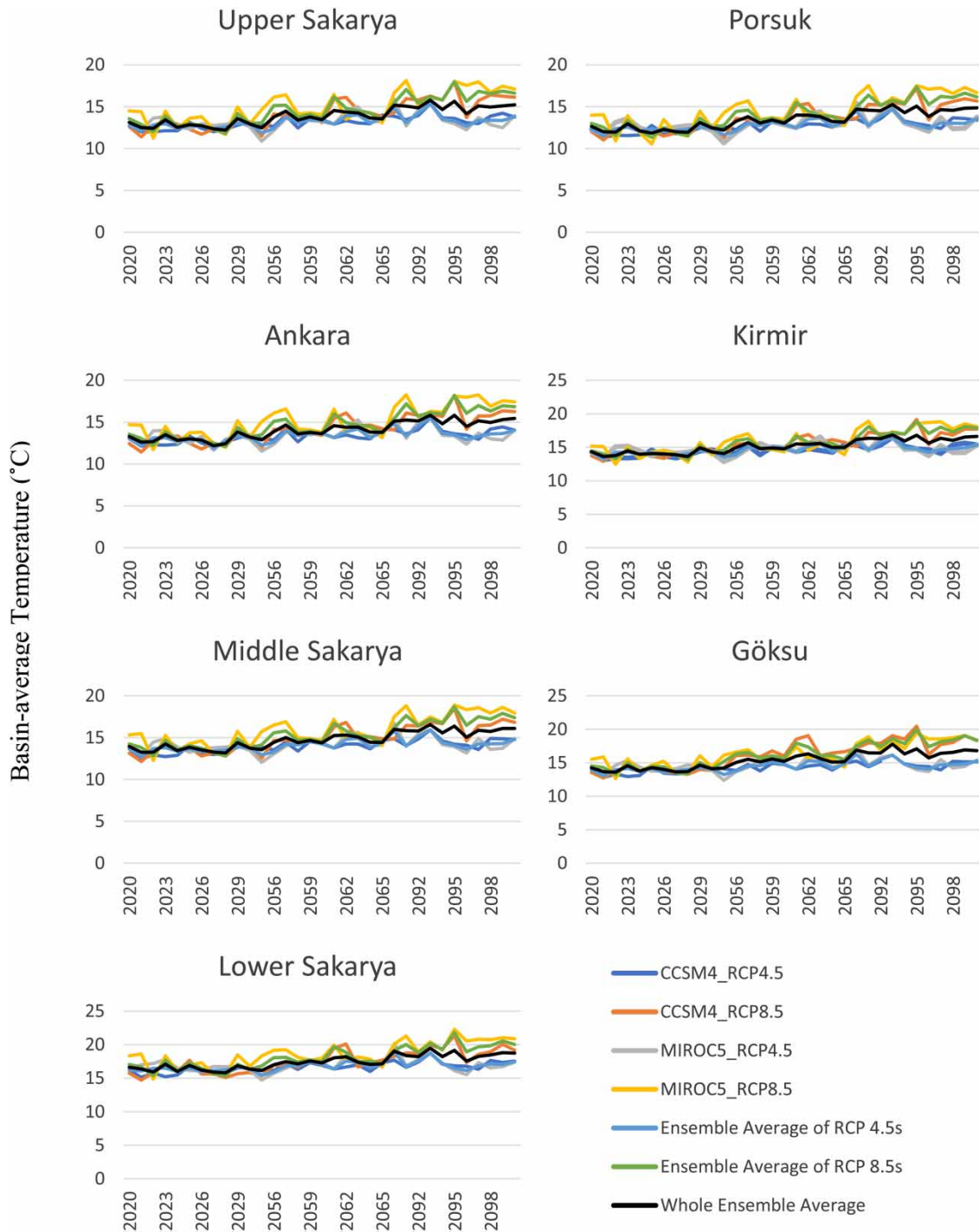


Figure 7 | Basin-average temperature over the following seven subbasins: Upper Sakarya, Porsuk, Ankara, Kirmir, Middle Sakarya, Göksu, Lower Sakarya. All four climate projection realizations, the ensemble averages of RCP 4.5 scenarios, the ensemble averages of RCP 8.5 scenarios, and the ensemble averages of all realizations are shown.

means of each future-period segment. Additionally, in the Supplementary Material, Figure B2 in Appendix B presents box-and-whisker plots of average monthly temperatures for the ensemble average across each subbasin.

In the Upper Sakarya subbasin, all climate projection realizations show an increasing trend in the 21st century. Moreover, except for MIROC5_RCP4.5, all of these trends are statistically significant. When each 11-year future-period segment is

analyzed individually, however, none of the trends have statistically meaningful p -values. It is also seen that there are climate projections with a decreasing trend. For instance, MIROC5 and the ensemble average of RCP 8.5 scenarios project a decreasing trend in the near century. In the mid-century, MIROC5_RCP4.5 is the only climate projection with a decreasing trend. Finally in the far century, MIROC5_RCP4.5, the ensemble of RCP 4.5 scenarios, and the ensemble of all GCMs have a decreasing trend. When the mean of the historical temperatures is compared with the mean of the future climate projections, it is seen that all future projections have higher means. The increase in the projected annual average temperatures ranges between 0.25 and 4.77 °C. The largest increase is projected by MIROC5_RCP8.5 in the far century while the lowest belongs to the CCSM4_RCP4.5 projection in the near century.

In the Porsuk subbasin, all climate projections point to rising temperatures for the entire 21st century. In addition, all these trends are statistically significant. In the near century, the only statistically significant increasing trend belongs to CCSM4_RCP4.5. Moreover, MIROC5_RCP8.5 and the ensemble average of RCP 8.5 scenarios show a decreasing trend. In the mid-century, there is no statistically meaningful trend. One of the climate projections, MIROC5_RCP8.5, points to a decreasing trend. Similar to the mid-century, none of the projections has a statistically important p -value in the far century. Three of these projections, namely CCSM4_RCP4.5, MIROC5_RCP4.5, and the ensemble of RCP 4.5 scenarios, have a decreasing trend. The average of the basin-scale temperatures for the historical period is always smaller than the future projections. The increase in the temperatures ranges between 0.24 and 4.86 °C. The lowest and the largest increase in the temperature is projected by CCSM4_RCP4.5 in the near century and MIROC5_RCP8.5 in the far century, respectively.

In the Ankara subbasin, temperatures are projected to increase in all climate projections for the entire 21st century. Except for MIROC5_RCP4.5, all climate projections have a statistically significant p -value. In the other future-period segments, however, none of the trends are statistically significant. In the near century, all MIROC5 projections show a decreasing trend while all other projections have an increasing trend. In the mid-century, the only projection with a decreasing trend is MIROC5_RCP8.5. Finally in the far century, MIROC5_RCP4.5 and the ensemble of RCP 4.5 scenarios have a decreasing trend. The mean values of all projections are always above the mean of the historical period. The range of the increase is between 0.20 and 4.78 °C, which are projected by CCSM4_RCP8.5 in the near century and by MIROC5_RCP8.5 in the far century, respectively.

In the Kirmir subbasin, the temperatures show an increasing trend throughout the 21st century. All of the climate projections except MIROC5_RCP4.5 have a trend line with a statistically significant p -value for the entire century. In the near, mid-, and far century, none of the projections has a statistically meaningful trend. In the near and mid-century, one of the projections, i.e., MIROC5_RCP8.5, has a decreasing trend. In the far century, CCSM4_RCP4.5, MIROC5_RCP4.5, and the ensemble of RCP 4.5 scenarios show a decreasing trend. The change in the average annual temperatures compared with the historical period ranges between -0.26 and 4.33 °C. The only decrease in the mean values is projected by MIROC5_RCP8.5 in the near century. The largest increase, on the other hand, also belongs to MIROC5_RCP8.5 but it is projected in the far century.

In the Middle Sakarya subbasin, all of the climate projections point to increasing temperatures in the 21st century. Furthermore, all of them except MIROC5_RCP4.5 have a statistically significant upward trend for the entire century. In the near century, MIROC5_RCP8.5 and the ensemble average of RCP 8.5 scenarios have downward trends. However, none of the trends are statistically important in this period. In the mid-century, there is only one projection with a significant p -value, which is CCSM4_RCP8.5. All of the projections except MIROC5_RCP8.5 have an upward trend. Finally, similar to the mid-century, there is no statistically significant trend in the far century. Three of the projections, i.e., CCSM4_RCP4.5, MIROC5_RCP4.5, and the ensemble of RCP 4.5 scenarios, have a downward trend. The mean values of the climate projections are always higher than the mean of the historical temperatures. The change in the mean values ranges between 0.22 and 4.89 °C. The lowest change belongs to CCSM4_RCP4.5 in the near century while the highest is in MIROC5_RCP8.5 in the far century.

In the Göksu subbasin, all climate projections show an upward trend in temperature with statistically significant p -values for the entire 21st century. Other 11-year future-period segments, however, do not have a statistically meaningful upward or downward trend. In the near century, MIROC5_RCP8.5 and the ensemble average of RCP 8.5 scenarios show a decreasing trend. In the mid-century, the only projection having a downward trend is MIROC5_RCP8.5. In the far century, the number of projections with a downward trend is higher as compared with the ones with an upward trend. Although there are projections with a downward trend, the mean values of these projections are always higher than the mean of the historical temperatures. The change ranges between 0.09 and 4.86 °C. The smallest and the largest increases belong to CCSM4_RCP4.5 in the near century and MIROC5_RCP8.5 in the far century, respectively.

In the Lower Sakarya subbasin, the basin-average temperature has an increasing trend for the entire 21st century. All of the trends except MIROC5_RCP4.5 are statistically significant. In the near, mid-, and far centuries, there is no statistically significant trend. In the near century, almost all of the projections except CCSM4_RCP4.5 and the ensemble average of RCP 4.5 scenarios have a decreasing trend. In the mid-century, however, MIROC5_RCP8.5 is the only projection with a downward trend. In the far century, CCSM4_RCP8.5, MIROC5_RCP8.5 and the ensemble of RCP 8.5 scenarios have an increasing trend, even though there are several projections with a downward trend, and the mean values of the projections in any segment of the future period are higher as compared with the historical period. The range of variation in basin-average temperatures is between 0.04 and 4.72 °C. As in almost all subbasins, the lowest change increase in the temperature is projected to be in CCSM4_RCP4.5 in the near century while the highest is in MIROC5_RCP8.5 in the far century.

The results show that for the most part the temperatures are increasing in all subbasins with significant *p*-values for the entire 21st century. In the near, mid-, and far century, although the trends are either downward or upward depending on the GCM and the RCP involved, the average of the basin-scale temperatures for all periods are always higher than the mean of the temperatures in the historical period. The only exception to that is Kirmir subbasin where the mean of the MIROC5_RCP8.5 projection in the near century is lower compared with the historical mean. Moreover, it is understood that the estimated increases in temperatures in RCP 8.5 scenarios are higher than in RCP 4.5 scenarios. This is most probably due to the fact that RCP 8.5 is a scenario of comparatively high GHG emissions while RCP 4.5 is an intermediate stabilization emission scenario. In addition, the lowest and highest increases in the temperatures in all subbasins are always projected by CCSM4_RCP4.5 and MIROC5_RCP8.5, respectively.

3.3. Predicted WEFE nexus vulnerability in the seven study subbasins considering climate and socio-economic factors

This section presents predictions for WEFE nexus sector vulnerabilities based on future climate changes and the selected indicators in the seven study subbasins. Table 6 presents the socio-economic indicator values and 21st-century climate trends for the study subbasins. Table 7 provides a summary of WEFE nexus sector vulnerability predictions and compares the seven study subbasins based on their vulnerabilities in terms of water, energy, food, and ecosystem sectors, which are represented by municipal water demand coverage, energy generation, agricultural productivity, and environmental flows, respectively. In the table, H, M, and L represent High, Moderate, and Low vulnerability, respectively. The following paragraphs detail the reasoning behind nexus sector vulnerability predictions for each subbasin.

The Upper Sakarya subbasin has a high percentage of agricultural areas (69.4%) and a relatively low population, but its economy heavily relies on agriculture. Decreasing precipitation trends in the 21st century could put pressure on the already

Table 6 | Socio-economic indicator values and 21st-century climate trends for study subbasins

	Agricultural areas (%)	Population	Industrial gross domestic product^a (million TL)	Current state river flow (hm³/y)	Annual average hydroelectric generation (GWh)	Annual average thermal electricity generation (GWh)	21st-century precipitation trend^b	21st-century temperature trend^b
Upper Sakarya	69.4	416,622	26.273 (Konya)	722	–	198	Decreasing	Increasing
Porsuk	50.4	1,002,397	26.273 (Eskişehir)	256	–	4,008	Decreasing	Increasing
Ankara/Kirmir	64.2/32.6	4,572,464/94,775	83.019 (Ankara)	432/371	–	6,141	Decreasing	Increasing
Middle Sakarya	31.6	343,357	6.586 (Bilecik)	838	1,388	6,633	Decreasing	Increasing
Göksu	49.8	288,985	81.188 (Bursa)	564	126	179	Decreasing	Increasing
Lower Sakarya	50.3	805,421	23.643 (Sakarya)	2,048	173	16,059	Decreasing	Increasing

^aFor the gross domestic product indicator, the value of the largest province in terms of population within the borders of the subbasin was used

^bBolded text means the trend is statistically significant. The trends were calculated for this study based on our methodological approach, as detailed in section 2.2.

Table 7 | Foresight on WEFE nexus sector vulnerabilities based on future climatic changes in seven study subbasins

Subbasin	Agricultural Productivity	Municipal Water Demand Coverage	Energy Generation	Environmental Flow
Upper Sakarya	H	M	L	M
Porsuk	M	H	M	H
Ankara	H	H	M	H
Kirmir	M	M	L	M
Middle Sakarya	M	M	H	H
Göksu	M	L	L	M
Lower Sakarya	M	L	M	M

H: High vulnerability; M: Moderate vulnerability; L: Low vulnerability

limited water resources, potentially leading to water scarcity and reduced crop yields. This scarcity could cascade across sectors: as agricultural productivity declines, economic pressures on farming communities could increase, and competition for water among sectors may intensify. Rising temperatures are expected to further drive water demand for both irrigation and cooling, compounding water scarcity and placing additional stress on farmers who depend on reliable water sources. Thus, agricultural productivity holds a high vulnerability rating in this subbasin. Municipal water demand coverage was assigned a moderate vulnerability level due to the absence of densely populated cities, suggesting current water supply infrastructure may suffice, though this could change with climate-driven pressures on the water supply. There is no hydroelectric power plant, and there is only one thermal power plant in the Upper Sakarya subbasin and therefore, energy generation has low vulnerability due to minimal dependence on large-scale water resources for energy production. However, the ecosystem sector exhibits moderate vulnerability due to agricultural activities. As environmental flows are likely to be impacted, especially during peak irrigation months, there is a risk of reduced water availability for natural habitats, potentially leading to ecological stress and loss of biodiversity.

The Porsuk subbasin has a moderate percentage of agricultural areas (50.4%) and a high population density, with an economy comparable to that of Upper Sakarya, also largely dependent on agriculture. Projected decreases in precipitation could result in water scarcity and reduced crop yields, directly affecting food security and impacting the local economy. High population density in Porsuk intensifies water demand, creating greater competition for limited resources, which may further strain water availability and amplify scarcity issues. Rising temperatures are expected to elevate water demand for household and industrial cooling, compounding pressures on the water sector and further stressing municipal supply systems. Additionally, reduced river flows could disrupt thermal power generation, posing potential risks to the energy sector and adding economic strain due to energy shortfalls. Agricultural productivity was assigned a moderate vulnerability level since the percentage of agricultural areas is moderate. However, municipal water demand coverage is expected to face high vulnerability due to the high population and, consequently, elevated water demand, indicating a substantial risk of water scarcity, especially during peak usage periods. While there is no hydroelectric generation in Porsuk, the presence of thermal power plants, some with dry-cooling systems, results in a moderate vulnerability rating for the energy sector. These plants are still susceptible to the impacts of reduced water availability on thermal power generation, as many rely on cooling water to maintain efficiency, meaning any decrease in river flow may have economic and operational consequences. Finally, the ecosystem sector has been assigned a high vulnerability rating due to the combined presence of agricultural and industrial activities. These activities may exert significant environmental pressures, potentially leading to ecological degradation and risks to biodiversity. Reduced environmental flows could compromise natural habitats, particularly during periods of increased water use for agriculture and industry.

The Ankara subbasin has the highest population density among the seven subbasins, with both agriculture and industry being key to its economy. As part of the province of Ankara, Türkiye's second most populous city and a major industrial hub within the Sakarya Basin, this subbasin plays a crucial role in regional resource demand. The nearby Kirmir subbasin serves as a vital drinking-water source, with water transfers from Kirmir's dams supplementing Ankara's water supply. However, persistent droughts have already limited Ankara's water resources, necessitating additional transfers from the Kızılırmak Basin. Decreasing precipitation trends could exacerbate water shortages, creating substantial pressure on agricultural

productivity, municipal water supplies, and environmental flows. Rising temperatures would further intensify water demand for household and industrial cooling, compounding these pressures. The Ankara subbasin's vulnerability is underscored by its high reliance on agriculture, particularly in Polatlı, Türkiye's 'granary', justifying a high vulnerability rating for agricultural productivity. Municipal water demand coverage is also rated highly vulnerable due to the large population's drinking-water needs. While hydroelectric power is absent, the thermal power plants in the region use wet-cooling systems, leading to a moderate vulnerability rating in electricity generation. Intense agricultural and industrial activity also raises environmental flow vulnerability to a high level, as these sectors heavily rely on water resources. In contrast, the Kirmir subbasin shows lower vulnerability across WEFE sectors due to fewer high-impact stressors, though decreased precipitation and increased temperatures are expected to strain its water resources over time.

The Middle Sakarya subbasin stands out with its hydroelectric production. There are tens of both dam and river-type hydroelectric power plants located on the Sakarya River main branch. The decreasing trend in precipitation depths can cause a reduction in water availability for energy production, leading to a reduction in electricity generation. In the Middle Sakarya subbasin, agricultural productivity and municipal water demand coverage were assigned moderate vulnerability levels since the share of agricultural areas (31.6%) is moderate and the subbasin has a low population density in comparison with the other subbasins. Electricity generation is highly dependent on water availability in the subbasin, and hence it has a high vulnerability rating. Finally, the environmental flow was assigned a high vulnerability rating since the presence of numerous hydroelectric production facilities in the subbasin can have a significant impact, especially under the changing climate.

In the Göksu and Lower Sakarya subbasins, while there is no statistically significant trend in precipitation, rising temperatures are expected to place increasing pressure on water availability, especially during the growing season, potentially impacting both food production and energy generation. Higher temperatures may lead to elevated evapotranspiration rates, which could increase water demand for irrigation, thereby affecting agricultural productivity. In the energy sector, temperature-driven increases in demand for water in thermal power generation could exacerbate resource competition, especially during dry periods. These factors collectively contribute to a low-to-moderate vulnerability level for the WEFE nexus sectors in these subbasins.

In this study, we analyzed future trends in precipitation and temperature to estimate the vulnerabilities of the WEFE nexus sectors. This paper is novel in its integration of high-resolution climate projections, a multi-indicator evaluation method, and a subbasin-specific approach to assess the impacts of climate change on the vulnerability of the WEFE nexus in a semi-arid watershed. However, it is important to acknowledge that vulnerability levels may vary due to many other factors that were not considered in this study. For example, agricultural productivity could be influenced by soil type, irrigation methods, and crop type, which were not examined. The vulnerability level of the energy sector can be affected by various factors such as the choice of renewable energy, the preference for dry-cooling systems in thermal power plants, and the prevention of evaporation losses in hydroelectric power plants. Additionally, the resilience of the water sector to climate change can be improved through sustainable practices such as preventing loss and leakage in water supply systems and reusing treated wastewater. The implementation of these practices can also contribute to improving the environmental flow. However, it is important to note that a holistic approach that considers the interdependencies between the water, energy, food, and ecosystem sectors and the impacts of climate change is necessary for sustainable development and the long-term resilience of the regions.

4. SUMMARY AND CONCLUSIONS

This study has found a general trend of decreasing precipitation in most subbasins of the Sakarya Basin during the 21st century, with Göksu and Lower Sakarya showing different patterns. While some increases are projected in Porsuk, Ankara, and Kirmir, most subbasins are expected to experience statistically significant declines. Meanwhile, temperatures are projected to rise across all subbasins, with the largest increases expected under the RCP 8.5 scenario, particularly in the MIROC5_RCP8.5 model.

These results highlight that climate-change impacts can vary greatly even within the same basin, depending on each subbasin's location and topography. This means that it is important to study each subbasin separately, especially in areas with diverse climates and terrains. Additionally, the differences observed between various climate models suggest that using multiple models is crucial to getting a more reliable picture of future climate impacts.

Understanding these changes in precipitation and temperature is key to managing the WEFE nexus. A decrease in precipitation can lead to less water availability, affecting agriculture, energy production, and the health of ecosystems. Rising

temperatures might further complicate these issues by increasing water and energy demand, lowering crop yields, and making water scarcity worse. This interconnectedness shows why it is important to include climate projections in WEFE nexus studies to spot potential risks and plan effective responses.

To tackle these challenges, it could be helpful to explore new water management practices, such as improving water-use efficiency, using crops that can withstand climate change, and investing in renewable energy sources that use less water. Also, working together with local stakeholders can lead to more effective and customized adaptation strategies.

The findings from this study will be used to calibrate water–energy system models for each subbasin in the Sakarya Basin. These models will help identify opportunities, challenges, and potential conflicts within the WEFE nexus, leading to the creation of tailored adaptation strategies. By focusing on the specific needs of each subbasin, this approach aims to ensure that the WEFE nexus remains sustainable and resilient as the climate continues to change.

While this study provides valuable insights into the climate-change impacts on the WEFE nexus in the Sakarya Basin, further advancements could enhance the robustness of such assessments. Our methodology currently utilizes two GCMs and two emission scenarios due to computational power and time constraints; however, increasing the number of GCMs and scenarios could further strengthen the analysis. Additionally, while we used CMIP5 data, given its availability for the study period, recent research is increasingly relying on CMIP6 projections. Future studies may consider CMIP6 data to provide even more up-to-date climate projections.

Furthermore, watershed characteristics in this study were quantified through specific indicators. For a more comprehensive vulnerability assessment, a deterministic model could be applied to simulate the watershed and evaluate water availability. We also based our analysis on historical socio-economic data under a ‘business-as-usual’ assumption, presuming stable socio-economic conditions. Future studies could benefit from examining how socio-economic factors might evolve under different scenarios, allowing for a more dynamic understanding of potential impacts on the WEFE nexus.

Overall, the findings of this study are expected to serve as a valuable guide for decision-makers involved in long-term planning within the Sakarya Basin and similar regions. By providing a detailed understanding of projected climate impacts on nexus sectors, these results offer a foundation for developing proactive, evidence-based strategies that address future water scarcity, agricultural productivity, energy generation, and ecosystem health. The subbasin-specific insights can inform adaptive management practices helping policymakers and stakeholders implement targeted interventions that enhance resilience across the WEFE nexus in the face of ongoing climate change.

ACKNOWLEDGEMENTS

We would like to acknowledge the Scientific and Technological Research Council of Türkiye (TÜBİTAK) for providing funding for the projects ‘Evaluation of Water, Energy and Food Nexus in Sakarya Watershed’ (project number 116Y166) and ‘A New Approach for Sustainable Water Management: Integration of the Circular Economy Approach to the Framework of Water–Energy–Food–Ecosystem Nexus’ (project number 121R014). We are also grateful to The Turkish Fulbright Commission for making this study possible with a visiting student researcher scholarship. Additionally, we would like to express our gratitude to Dr Ali Ercan for his invaluable guidance and support during this research at the UC Davis Hydrologic Research Lab.

FUNDING

This work was supported by the Scientific and Technological Research Council of Türkiye (TÜBİTAK) [grant numbers 116Y166 and 121R014].

DATA AVAILABILITY STATEMENT

All relevant data are included in the paper or its Supplementary Information.

CONFLICT OF INTEREST

The authors declare there is no conflict.

REFERENCES

- Alakbar, T. & Burgan, H. I. (2024) Regional power duration curve model for ungauged intermittent river basins, *J. Water Clim. Chang.*, **15**, 4596–4612. <https://doi.org/10.2166/wcc.2024.207>.
- Albatayneh, A. (2023) Water energy food nexus to tackle climate change in the eastern Mediterranean, *Air, Soil Water Res.*, **16**. <https://doi.org/10.1177/11786221231170222>.
- Apeh, O. O. & Nwulu, N. I. (2024) The water–energy–food–ecosystem nexus scenario in Africa: perspective and policy implementations, *Energy Reports*, **11**, 5947–5962. <https://doi.org/10.1016/j.egy.2024.05.060>.
- Baccour, S., Albiac, J., Ward, F., Kahil, T., Esteban, E., Uche, J., Calvo, E. & Crespo, D. (2024) Managing climate risks: new evidence from integrated analysis at the basin scale, *Int. J. Water Resour. Dev.*, **40**, 915–939. <https://doi.org/10.1080/07900627.2024.2390937>.
- Bates, B. C., Kundzewicz, Z. W., Wu, S. & Palutikof, J. P. (2008) Climate change and water resources in systems and sectors. In: Bates, B. C., Kundzewicz, Z. W., Wu, S. & Palutikof, J. P. (eds) *Climate Change and Water*. Geneva, Switzerland: IPCC Secretariat, pp. 53–76.
- Cevik, S. (2022) *Climate Change and Energy Security: The Dilemma or Opportunity of the Century?*, IMF Working Paper WP/22/174, Washington, DC, USA: International Monetary Fund. <https://doi.org/10.5089/9798400218347.001>.
- Dlamini, N., Senzanje, A. & Mabhaudhi, T. (2023) The water–energy–food (WEF) nexus as a tool to develop climate change adaptation strategies: a case study of the Buffalo River catchment, South Africa, *J. Water Clim. Chang.*, **14**, 4465–4488. <https://doi.org/10.2166/wcc.2023.263>.
- Dong, G., Xie, Y., Wang, Y., Fan, D. & Tian, Z. (2021) Ensemble projection of extreme precipitation over China based on three dynamical downscaling simulations, *Front. Earth Sci.*, **9**, 755041. <https://doi.org/10.3389/feart.2021.755041>.
- DSİ (2017) *Sakarya Havzası Master Plan Nihai Raporu*. Eskişehir, Turkey: Orman ve Su İşleri Bakanlığı Devlet Su İşleri Genel Müdürlüğü 3. Bölge Müdürlüğü.
- DSİ (2022) HES Su Kullanım Anlaşmaları [WWW Document]. Yenilenebilir Enerji Dairesi Başkanlığı. Available at: <https://enerji.dsi.gov.tr/Sayfa/Detay/774> (accessed 12.6.22).
- Dudhia, J. (1989) Numerical study of convection observed during the Winter Monsoon Experiment using a mesoscale two-dimensional model, *J. Atmos. Sci.*, **46**, 3077–3107. [https://doi.org/10.1175/1520-0469\(1989\)046<3077:NSOCOD>2.0.CO;2](https://doi.org/10.1175/1520-0469(1989)046<3077:NSOCOD>2.0.CO;2).
- Dulière, V., Zhang, Y. & Salathé, E. P. (2011) Extreme precipitation and temperature over the U.S. Pacific Northwest: a comparison between observations, reanalysis data, and regional models, *J. Clim.*, **24**, 1950–1964. <https://doi.org/10.1175/2010JCLI3224.1>.
- Endo, A., Burnett, K., Orencio, P. M., Kumazawa, T., Wada, C. A., Ishii, A., Tsurita, I. & Taniguchi, M. (2015) Methods of the water–energy–food nexus, *Water*, **7**, 5806–5830. <https://doi.org/10.3390/w7105806>.
- Enerji Atlası (2023) Enerji Atlası [WWW Document]. Available at: <http://www.enerjiatlası.com/> (accessed 2.16.23).
- Erler, A. R., Peltier, W. R. & D'Orgeville, M. (2015) Dynamically downscaled high-resolution hydroclimate projections for western Canada, *J. Clim.*, **28**, 423–450. <https://doi.org/10.1175/JCLI-D-14-00174.1>.
- European Environment Agency (EEA) (2018) CORINE Land Cover 2018 [WWW Document]. Available at: <https://land.copernicus.eu/en/products/corine-land-cover/clc2018> (accessed 12.20.24).
- FAO (2015) *Climate Change and Food Security: Risks and Responses*. Rome, Italy: Food and Agriculture Organization of the United Nations.
- Gao, S., Huang, D., Du, N., Ren, C. & Yu, H. (2022) WRF ensemble dynamical downscaling of precipitation over China using different cumulus convective schemes, *Atmos. Res.*, **271**, 106116. <https://doi.org/10.1016/j.atmosres.2022.106116>.
- Gao, D., Chen, A. S. & Memon, F. A. (2024) A systematic review of methods for investigating climate change impacts on Water–Energy–Food nexus, *Water Resources Management*, **38**, 1–43. <https://doi.org/10.1007/s11269-023-03659-x>.
- Garcia, D. J., Lovett, B. M. & You, F. (2019) Considering agricultural wastes and ecosystem services in Food–Energy–Water–Waste Nexus system design, *J. Clean. Prod.*, **228**, 941–955. <https://doi.org/10.1016/j.jclepro.2019.04.314>.
- Gent, P. R., Danabasoglu, G., Donner, L. J., Holland, M. M., Hunke, E. C., Jayne, S. R., Lawrence, D. M., Neale, R. B., Rasch, P. J., Vertenstein, M., Worley, P. H., Yang, Z. L. & Zhang, M. (2011) The Community Climate System Model version 4, *J. Clim.*, **24**, 4973–4991. <https://doi.org/10.1175/2011JCLI4083.1>.
- Giorgi, F. & Bates, G. T. (1989) The climatological skill of a regional model over complex terrain, *Mon. Weather Rev.*, **117**, 2325–2347. [https://doi.org/10.1175/1520-0493\(1989\)117<2325:TCOAR>2.0.CO;2](https://doi.org/10.1175/1520-0493(1989)117<2325:TCOAR>2.0.CO;2).
- Giorgi, F. & Gutowski, W. J. (2015) Regional dynamical downscaling and the CORDEX initiative, *Annu. Rev. Environ. Resour.*, **40**, 467–490. <https://doi.org/10.1146/annurev-environ-102014-021217>.
- Giupponi, C. & Gain, A. K. (2017) Integrated spatial assessment of the water, energy and food dimensions of the Sustainable Development Goals, *Reg. Environ. Chang.*, **17**, 1881–1893. <https://doi.org/10.1007/s10113-016-0998-z>.
- Gorguner, M., Kavvas, M. L. & Ishida, K. (2019) Assessing the impacts of future climate change on the hydroclimatology of the Gediz Basin in Turkey by using dynamically downscaled CMIP5 projections, *Sci. Total Environ.*, **648**, 481–499. <https://doi.org/10.1016/j.scitotenv.2018.08.167>.
- Grell, G. A. & Dévényi, D. (2002) A generalized approach to parameterizing convection combining ensemble and data assimilation techniques, *Geophys. Res. Lett.*, **29** (14), 381–384. <https://doi.org/10.1029/2002GL015311>.
- Hanes, R. J., Gopalakrishnan, V. & Bakshi, B. R. (2018) Including nature in the food–energy–water nexus can improve sustainability across multiple ecosystem services, *Resour. Conserv. Recycl.*, **137**, 214–228. <https://doi.org/10.1016/j.resconrec.2018.06.003>.

- Hay, L. E. & Clark, M. P. (2003) Use of statistically and dynamically downscaled atmospheric model output for hydrologic simulations in three mountainous basins in the western United States, *J. Hydrol.*, **282**, 56–75. [https://doi.org/10.1016/S0022-1694\(03\)00252-X](https://doi.org/10.1016/S0022-1694(03)00252-X).
- Hong, S. Y., Noh, Y. & Dudhia, J. (2006) A new vertical diffusion package with an explicit treatment of entrainment processes, *Mon. Weather Rev.*, **134**, 2318–2341. <https://doi.org/10.1175/MWR3199.1>.
- Hu, X. M., Xue, M., McPherson, R. A., Martin, E., Rosendahl, D. H. & Qiao, L. (2018) Precipitation dynamical downscaling over the great plains, *J. Adv. Model. Earth Syst.*, **10**, 421–447. <https://doi.org/10.1002/2017MS001154>.
- Ishida, K., Gorguner, M., Ercan, A., Trinh, T. & Kavvas, M. L. (2017) Trend analysis of watershed-scale precipitation over northern California by means of dynamically-downscaled CMIP5 future climate projections, *Sci. Total Environ.*, **592**, 12–24. <https://doi.org/10.1016/j.scitotenv.2017.03.086>.
- Ishida, K., Ercan, A., Trinh, T., Jang, S., Kavvas, M. L., Ohara, N., Chen, Z. Q., Kure, S. & Dib, A. (2020) Trend analysis of watershed-scale annual and seasonal precipitation in northern California based on dynamically downscaled future climate projections, *J. Water Clim. Chang.*, **11**, 86–105. <https://doi.org/10.2166/wcc.2018.241>.
- Jander, V., Vicuña, S., Melo, O. & Lorca, Á. (2023) Adaptation to climate change in basins within the context of the water–energy–food nexus, *J. Water Resour. Plan. Manag.*, **149**, 04023060. [https://doi.org/10.1061/\(asce\)he.1943-5584.0000939](https://doi.org/10.1061/(asce)he.1943-5584.0000939).
- Jang, S. & Kavvas, M. L. (2015) Downscaling global climate simulations to regional scales: statistical downscaling versus dynamical downscaling, *J. Hydrol. Eng.*, **20**, A4014006. [https://doi.org/10.1061/\(asce\)he.1943-5584.0000939](https://doi.org/10.1061/(asce)he.1943-5584.0000939).
- Karabulut, A. A., Udias, A. & Vigiak, O. (2019) Assessing the policy scenarios for the Ecosystem Water Food Energy (EWFE) nexus in the Mediterranean region, *Ecosyst. Serv.*, **35**, 231–240. <https://doi.org/10.1016/j.ecoser.2018.12.013>.
- Kaur, M., Krishna, R. P. M., Joseph, S., Dey, A., Mandal, R., Chattopadhyay, R., Sahai, A. K., Mukhopadhyay, P. & Abhilash, S. (2020) Dynamical downscaling of a multimodel ensemble prediction system: application to tropical cyclones, *Atmos. Sci. Lett.*, **21**, e971. <https://doi.org/10.1002/asl.971>.
- Kessler, E. (1969) *On the Distribution and Continuity of Water Substance in Atmospheric Circulations*. Boston, MA, USA: American Meteorological Society.
- Kim, J. W., Chang, J. T., Baker, N. L., Wilks, D. S. & Gates, W. L. (1984) The statistical problem of climate inversion: determination of the relationship between local and large-scale climate, *Mon. Weather Rev.*, **112**, 2069–2077. [https://doi.org/10.1175/1520-0493\(1984\)112<2069:TSPOCI>2.0.CO;2](https://doi.org/10.1175/1520-0493(1984)112<2069:TSPOCI>2.0.CO;2).
- Komurcu, M., Emanuel, K. A., Huber, M. & Acosta, R. P. (2018) High-resolution climate projections for the northeastern United States using dynamical downscaling at convection-permitting scales, *Earth Sp. Sci.*, **5**, 801–826. <https://doi.org/10.1029/2018EA000426>.
- Latif, M. (2011) Uncertainty in climate change projections, *J. Geochemical Explor.*, **110**, 1–7. <https://doi.org/10.1016/j.gexplo.2010.09.011>.
- Liu, Q. (2016) Interlinking climate change with water–energy–food nexus and related ecosystem processes in California case studies, *Ecol. Process.*, **5**, 14. <https://doi.org/10.1186/s13717-016-0058-0>.
- Mann, H. B. (1945) Nonparametric tests against trend, *Econometrica*, **13**, 245–259. <https://doi.org/10.2307/1907187>.
- Maraun, D. (2016) Bias correcting climate change simulations – a critical review, *Curr. Clim. Chang. Reports*, **2**, 211–220. <https://doi.org/10.1007/s40641-016-0050-x>.
- Mlawer, E. J., Taubman, S. J., Brown, P. D., Iacono, M. J. & Clough, S. A. (1997) Radiative transfer for inhomogeneous atmospheres: RRTM, a validated correlated-k model for the longwave, *J. Geophys. Res. Atmos.*, **102**, 16663–16682. <https://doi.org/10.1029/97jd00237>.
- Momblanch, A., Papadimitriou, L., Jain, S. K., Kulkarni, A., Ojha, C. S. P., Adelaye, A. J. & Holman, I. P. (2019) Untangling the water–food–energy–environment nexus for global change adaptation in a complex Himalayan water resource system, *Sci. Total Environ.*, **655**, 35–47. <https://doi.org/10.1016/j.scitotenv.2018.11.045>.
- Nhamo, L., Mabhauthi, T., Mpandeli, S., Dickens, C., Nhemachena, C., Senzanje, A., Naidoo, D., Liphadzi, S. & Modi, A. T. (2020) An integrative analytical model for the water–energy–food nexus: South Africa case study, *Environmental Science & Policy*, **109**, 15–24. <https://doi.org/10.1016/j.envsci.2020.04.010>.
- Özcan, Z. (2023) *A Holistic Framework for Evaluating the Sustainability of the Water–Energy–Food–Ecosystem Nexus under Multiple Socioeconomic and Climate Change Conditions*. PhD thesis. Middle East Technical University.
- Riahi, K., Rao, S., Krey, V., Cho, C., Chirkov, V., Fischer, G., Kindermann, G., Nakicenovic, N. & Rafaj, P. (2011) RCP 8.5 – a scenario of comparatively high greenhouse gas emissions, *Clim. Change*, **109**, 33–57. <https://doi.org/10.1007/s10584-011-0149-y>.
- Saladini, F., Betti, G., Ferragina, E., Bouraoui, F., Cupertino, S., Canitano, G., Gigliotti, M., Autino, A., Pulselli, F. M., Riccaboni, A., Bidoglio, G. & Bastianoni, S. (2018) Linking the water–energy–food nexus and sustainable development indicators for the Mediterranean region, *Ecol. Indic.*, **91**, 689–697. <https://doi.org/10.1016/j.ecolind.2018.04.035>.
- Skamarock, W. C., Klemp, J. B., Dudhia, J., Gill, D. O., Barker, D. M., Duda, M. G., Huang, X.-Y., Wang, W. & Powers, J. G. (2008) *A Description of the Advanced Research WRF Version 3*. NCAR Technical Note NCAR/TN-475+STR, Boulder, CO, USA: National Center for Atmospheric Research. <https://doi.org/10.5065/D68S4MVH>.
- Smirnova, T. G., Brown, J. M. & Benjamin, S. G. (1997) Performance of different soil model configurations in simulating ground surface temperature and surface fluxes, *Mon. Weather Rev.*, **125**, 1870–1884. [https://doi.org/10.1175/1520-0493\(1997\)125<1870:PODSMC>2.0.CO;2](https://doi.org/10.1175/1520-0493(1997)125<1870:PODSMC>2.0.CO;2).
- Soares, P. M. M., Cardoso, R. M., Miranda, P. M. A., de Medeiros, J., Belo-Pereira, M. & Espirito-Santo, F. (2012) WRF high resolution dynamical downscaling of ERA-Interim for Portugal, *Clim. Dyn.*, **39**, 2497–2522. <https://doi.org/10.1007/s00382-012-1315-2>.

- SYGM (2022) *Sakarya Havzası Nehir Havza Yönetim Planı Hazırlanması Projesi Stratejik Çevresel Değerlendirme Kapsam Belirleme Raporu*. Ankara, Turkey: T.C. Tarım ve Orman Bakanlığı Su Yönetimi Genel Müdürlüğü.
- T.C. Sanayi ve Teknoloji Bakanlığı (2020) 81 İl Sanayi Durum Raporları [WWW Document]. Available at: <https://www.sanayi.gov.tr/plan-program-raporlar-ve-yayinlar/81-il-sanayi-durum-raporlari> (accessed 5.4.23).
- The Ministry of Forestry and Water Affairs (2016) *İklim Değişikliğinin Su Kaynaklarına Etkisi Projesi Proje Nihai Raporu*. Ankara, Turkey: General Directorate of Water Management, The Ministry of Forestry and Water Affairs.
- Thomson, A. M., Calvin, K. V., Smith, S. J., Kyle, G. P., Volke, A., Patel, P., Delgado-Arias, S., Bond-Lamberty, B., Wise, M. A., Clarke, L. E. & Edmonds, J. A. (2011) RCP4.5: a pathway for stabilization of radiative forcing by 2100, *Clim. Change*, **109**, 77–94. <https://doi.org/10.1007/s10584-011-0151-4>.
- Van Khiem, M., Redmond, G., McSweeney, C. & Thuc, T. (2014) Evaluation of dynamically downscaled ensemble climate simulations for Vietnam, *Int. J. Climatol.*, **34**, 2450–2463. <https://doi.org/10.1002/joc.3851>.
- Watanabe, M., Suzuki, T., Oishi, R., Komuro, Y., Watanabe, S., Emori, S., Takemura, T., Chikira, M., Ogura, T., Sekiguchi, M., Takata, K., Yamazaki, D., Yokohata, T., Nozawa, T., Hasumi, H., Tatebe, H. & Kimoto, M. (2010) Improved climate simulation by MIROC5: mean states, variability, and climate sensitivity, *J. Clim.*, **23**, 6312–6335. <https://doi.org/10.1175/2010JCLI3679.1>.
- Wu, L., Elshorbagy, A. & Alam, M. S. (2022) Dynamics of water–energy–food nexus interactions with climate change and policy options, *Environ. Res. Commun.*, **4**, 015009. <https://doi.org/10.1088/2515-7620/ac4bab>.
- Wubneh, M. A., Worku, T. A. & Chekol, B. Z. (2023) Climate change impact on water resources availability in the Kiltie watershed, Lake Tana sub-basin, Ethiopia, *Heliyon*, **9**, e13941. <https://doi.org/10.1016/j.heliyon.2023.e13941>.
- Xu, Z., Han, Y. & Yang, Z. (2019) Dynamical downscaling of regional climate: a review of methods and limitations, *Sci. China Earth Sci.*, **62**, 365–375. <https://doi.org/10.1007/s11430-018-9261-5>.
- Yuan, M. H. & Lo, S. L. (2020) Developing indicators for the monitoring of the sustainability of food, energy, and water, *Renew. Sustain. Energy Rev.*, **119**, 109565. <https://doi.org/10.1016/j.rser.2019.109565>.

First received 27 August 2024; accepted in revised form 4 December 2024. Available online 19 December 2024